colloids and interfaces

MDPI

Article

Asphaltene Precipitation and the Influence of Dispersants and Inhibitors on Morphology Probed by AFM

Daniela Mojica [1], Mauricio Angeles [2], Oscar Alvarez [1] and Diego Pradilla [1,*]

[1] Department of Chemical and Food Engineering, Universidad de los Andes, Bogotá 111711, Colombia
[2] The Dow Chemical Company, Dow Química Mexicana S.A. de C.V., Av. Paseo de la Reforma 243, Piso 8, Ciudad de México 06500, Mexico
* Correspondence: d-pradil@uniandes.edu.co; Tel.: +57-601-339-4949 (ext. 3935)

Abstract: Bridging the gap between laboratory-scale experiments and actual oilfield operations is a complex task that requires a compromise between real (authentic) fluids and model systems. Commercial products (i.e., asphaltene inhibitors and dispersants) are often designed to target a wide range of operating conditions and compositions of crude oils, which means that the performance becomes almost case-specific. Through Atomic Force Microscopy (AFM) imaging and Transmission/Backscattering signals (T/BS), the morphology of asphaltene deposits and the mechanisms that eventually lead to precipitated material were evaluated. Two different models (starting solutions) with four different *n*-alkanes were used to induce variability in asphaltene agglomeration and subsequent precipitation paths. It was found that increasing the carbon number shifted the observed precipitation detection time (T/BS data suggested a shift in the order of $\sim$ 1000 s when comparing low and high carbon numbers) and influences the density of the precipitated material under static and a sufficiently high concentration of solvent conditions. Further analysis on the morphology of the resulting material after the addition of commonly used chemicals showed that asphaltene stability through inhibition (i.e., blockage or crowding of potential active sites) led to smaller complexes. One of the additives (PIBSA) reduced the average height in $\sim$ 33% and the mean square roughness in $\sim$ 72%. On the other hand, stability through dispersion (i.e., hindering agglomeration) leads to a polymer-like network bigger in size, noting that in both cases the system remains soluble. The use of APR resulted in an increase of $\sim$ 41% and $\sim$ 54% for the same parameters. This insight sheds light on how to devise efficient chemical strategies to prevent flow assurance issues.

Keywords: asphaltenes; precipitation; inhibitors; dispersants; kinetics; aggregation; stability

Citation: Mojica, D.; Angeles, M.; Alvarez, O.; Pradilla, D. Asphaltene Precipitation and the Influence of Dispersants and Inhibitors on Morphology Probed by AFM. *Colloids Interfaces* **2023**, *7*, 3. https://doi.org/10.3390/colloids7010003

Received: 27 September 2022
Revised: 4 November 2022
Accepted: 4 January 2023
Published: 10 January 2023

1. Introduction

Major challenges in the petroleum industry arise when processing, transport, refining and storage conditions allow asphaltene fractions to exhibit their interfacial properties and multiple colloidal interactions involving different surfaces/interfaces [1,2]. During extraction operations, these indigenous components of crude oil are known to aid in the formation and stabilization of water-in-crude oil (W/O) and crude oil-in-water (O/W) emulsions by forming a mechanically robust skin around the droplets [3–5]. During production, asphaltenes can alter the wettability of different surfaces by irreversible adsorption, making enhanced oil recovery processes more complex [6]. When significant changes in pressure are present, they can abruptly stabilize foams due to the sudden emergence of another phase in the foam lamellae, an undesirable situation [7]. In transportation, they are known to phase transition, precipitate and, if the pressure/temperature conditions are favorable, they can deposit at solid–liquid surfaces, forming layers that could eventually damage the inner lining of pipelines as well as create rigid plugs [8–10]. These events lead to flow assurance issues that negatively affect operational costs [11].

Attempts to prevent and mitigate the negative effects due to the presence of asphaltenes during transportation of crude oils include: (i) heating, where thermally insulated

pipelines and electrical heaters keep the fluid at a medium-to-high temperature to reduce viscosity and maintain the asphaltene fraction in a single phase. The main drawback is economic feasibility due to large power demands. (ii) Dilution, where other oil fractions such as naphtha, low molar mass *n*-alkanes and lighter oils are mixed with the main fluid to improve mobility and modify the asphaltene concentration. Although attractive as a strategy, the costs associated with the diluent tend to be high and the original properties of the extracted fluid are modified. (iii) Upgrading with synthetic oils, which is normally a costly operation. (iv) chemical treatments, where surface-active compounds known as inhibitors and dispersants are used to maintain asphaltenes in a type of colloidal stability, preventing precipitation and future deposition [12–15].

It is clear that the main issues related to asphaltenes, which eventually lead to flow assurance problems, are phase transition—that is, changes in pressure and temperature that draw asphaltenes out of solution and allow them to aggregate, precipitate and deposit [16,17]. Even though there are still areas open for discussion about the mechanisms behind self-association and phase transitions, there seems to be a consensus on the different steps that could result in a deposited asphaltene layer. These steps are, first, the destabilization of asphaltene monomers (nanoscale level) that allow them to keep growing in size by interacting with other monomers. The extent of the interaction is dominated by the solubility conditions of the media [18]. Second, a subsequent set of interactions that lead to a change in scale, that is, from the nanometer to the micrometer size. Third, the phase transition that occurs at the micrometer scale with an asphaltene aggregate or cluster when they are no longer stable in the bulk solution [19]. Finally, fourth, asphaltene aggregate adsorption onto a solid surface, a physical phenomenon that can be described through an equation of state or determined experimentally by measuring the adsorption enthalpy [20]. Evidently, these steps do not necessarily need to be sequential or chronological, meaning that asphaltene nanoaggregates or monomers, if present, do have the ability to adsorb and negatively impact flow assurance not only in transportation, but also during injection (porous media, pore throats) and production (lifting systems) [21,22]. Asphaltene monomers, though typically loosely bound, tend to follow kinetic-limited adsorption at short times, while aged networks at longer times seem to follow diffusion-limited models [23,24].

The processes and events that follow adsorption and that can eventually lead to a macroscopic asphaltene plug (e.g., in an oil pipeline) are diverse, but it is clear that the clusters increase in size under turbulent flow conditions possibly as a result of orthokinetic aggregation and a balance with the fragmentation that occurs through hydrodynamic stresses (shear) [25,26].

Asphaltene aggregation and self-association (under favorable and unfavorable solubility conditions) have been extensively studied using multiple techniques (optical microscopy, UV-Vis spectroscopy, ultrasmall-, small- and wide-angle scattering, refractive index measurements, quartz crystal resonator (QCR) High Resolution Transmission Electron Microscopy (HRTEM)) [27–33], indicating that the governing forces driving this phenomenon are primarily of the Van der Waals type, Hydrogen bonding, acid-base interactions and $\pi - \pi$ stacking [34–36]. The origin of these interactions is the nature of the asphaltene fraction, functionally defined in terms of solubility (soluble in aromatics but insoluble in *n*-alkanes) and the presence of multiple components (polyaromatic cores, metals, aliphatic chains, heteroatoms and functional groups such as hydroxyl, carbonyl, amine and nitrile, among others) that add to their molecular complexity [37–39].

Asphaltene precipitation studies have shown that slow kinetic aggregation plays an important role; however, long detection times make it difficult to establish accurate stability regions [40,41]. One possible explanation for this is the reduction of the free surface energy by self-association [42]. Geometric population balance equations have been used to obtain robust values for the Hildebrand solubility parameters and these results can be used as inputs for modeling parameters and better estimation of detection times [43–45]. Finally, asphaltene deposition and dynamics have been studied under a wide range of techniques such as capillary and Couette flow cells [46–48], quartz crystal microbalance measurements

(QCM, QCM-D) [22,49,50], calorimetry [20], Field Emission Scanning Electron Microscopy (FE-SEM) [51] and other apparatus [52]. For instance, Campen et al. [49] evaluated the behavior of an asphaltene inhibitor under favorable and unfavorable solubility conditions using QCM-D and found that the deposited mass is altered depending on the *n*-heptane volume fraction, suggesting a change from asphaltene flocs (60 vol%) to aggregates of the micrometer scale (80 vol%). Goual et al. [53] studied asphaltene aggregation under unfavorable solubility conditions (HepTol) and the influence of alkylphenols by means of HRTEM and molecular dynamics (MD). They showed differences in the morphology of the deposited material (e.g., from globular to filamentary), a decrease in the aggregate size after exposure time and a possible route of additive–asphaltene interaction through peripheral H-bonding. Furthermore, Goual and Sedghi [54] studied the effect of dodecylbenzenesulfonic acid (DBSA) on asphaltene aggregation using the same techniques and showed that DBSA interacts in a very different way compared to alkylphenols to form similar thick filaments.

The picture, however, remains incomplete. Some gaps need to be bridged, for instance: (i) the use of well-defined solid surfaces (e.g., gold) which are significantly different from uneven, aged pipelines made of other materials; (ii) the use of model solutions (e.g., toluene, HepTol) which do not fully capture the dynamics induced by authentic fluids made up of thousands, even millions, of different molecules (e.g., crude oil and crude oil solutions); and (iii) the lack of inclusion of high molecular weight polymer-like additives which are more common in the oil and gas industry than short alkyl-chain molecules.

For these reasons, field operations and experimental results at the laboratory scale need to be bridged by implementing the use of commercial products specifically made to meet different customer needs. In this study, the effect of a set of four commercially available inhibitors and dispersants on asphaltene precipitation and deposition was evaluated. Two different media for asphaltenes were assessed, one attempting to mimic a dilution strategy from a Colombian heavy crude oil and the second from a re-solubilized asphaltene extraction with different solvents. Atomic Force Microscopy (AFM) and transmission/backscattering signals were the main techniques used to follow the changes on morphology and colloidal stability of the systems.

2. Materials and Methods

A heavy crude oil with a high asphaltene content from a Colombian oilfield was used for asphaltene extraction and for model oil preparation. The main properties of this oil are listed in Table 1.

Table 1. Properties of the Colombian heavy crude oil used in this work.

Parameter	Method	Value
Saturates (%wt)	IP 469 [55]	7.4
Aromatics (%wt)		37.8
Resins (%wt)		15.3
Asphaltenes (%wt)		39.5
Density (kg/m^3) at 15.5 °C	ASTM D7042-19 [56]	954
Density (°API) at 15.5 °C	ASTM D7042-19 [56]	13.6
TAN (mg KOH/g)	ASTM D664-18e2 [57]	0.134

A set of four commercially available inhibitors/dispersants of different chemistry and architecture were purchased from Sigma Aldrich and used as received. The main properties of these compounds are listed on Table 2.

Asphaltene extraction. Asphaltenes were extracted following the standard procedure ASTM D 6560 [58]. In this method, C_7 asphaltenes are precipitated directly from crude oil by mixing it with *n*-heptane (Sigma Aldrich) in a 40:1 mass ratio. This mixture is mechanically stirred at ambient temperature for 24 h. The mixture is then vacuum filtered using a 0.45 µm HVLP (Millipore) membrane filter. Recovered asphaltenes are then put into a nitrogen atmosphere degasser and dried for 48 h. Solid asphaltenes were weighted every 12 h until

the mass was constant to ensure complete evaporation of *n*-heptane. The solid asphaltenes can then be dissolved in toluene to prepare the below-mentioned asphaltene solutions.

Table 2. Compounds used as inhibitors/dispersants.

Commercial Family (Name Used in this Work)	Molar Mass (Kg/mol)	Density (Kg/m^3)
Ethoxylated nonylphenol (ENP)	396	1027
Dodecylbenzene sulfonic acid (DBSA)	326	1060
Alkyl phenolic resin (APR)	>1200	900
Polyisobutylene succinic anhydride derivative (PIBSA)	>800	936

Solvents. To evaluate the effect of different solubility conditions in the final morphology and colloidal stability of asphaltenes, four *n*-alkanes were used, namely *n*-dodecane, *n*-decane, *n*-heptane and *n*-hexane (Sigma Aldrich). Additionally, toluene (Sigma Aldrich) was used as a diluent for crude oil.

Model systems. Two different model oil systems were built based on the required kinetics and mechanistic attributes depending on the starting conditions. It has been stated and observed that the so-called precipitation onset is somewhat arbitrary because it largely depends on the measured size (technique-dependent) of asphaltene clusters/aggregates and the nature of the precipitant [40,59,60]. This means that under different solubility conditions, the paths that the monomers take, the rate of growth and the total amount of precipitated material will be different. However, in the final state, a thermodynamic limit is reached, something that can be explained by combining the entropy of mixing the effects of molecules with different chemistry with the heat of mixing (e.g., Flory–Huggins model) [61]. Based on this and on previous oilfield procedures [62], the two model systems are as follows:

Model 1: A 0.5 mL aliquot of crude oil diluted in toluene (10%wt) is added to 10 mL of one of the four *n*-alkanes and manually shaken for 30 s.

Model 2: A 3 mL aliquot of an asphaltene solution in toluene (2 g/L) is added to 7 mL of *n*-heptane and manually shaken for 30 s.

Transmission and backscattering measurements. A Turbiscan Lab Stability Analyzer (Formulaction SA, Tolouse, France) was used to follow the transmission (0° from the incident light beam) and backscattering (135° from the incident light beam) signals from a pulsed near-infrared light source (λ = 850 nm). Measurements at ambient temperature (22 °C) were performed to assess the colloidal stability and extent of precipitation of the two models for up to 4 h. The Δ-backscattering value (%ΔBS) gives a relative qualitative measure of how much light hits the precipitated material (as it falls within the measuring vial) while the transmission (%ΔT) can be interpreted as how much light manages to go through the sample undisturbed. The instrument vertically scans the measurement vial along its height, recording data in 20 μm steps. The freshly prepared samples were introduced into the instrument vial and pulses every 25 s were taken to record the signals. Data on later sections will be displayed in terms of %ΔBS, %ΔT and height. The latter term corresponds to the relative position of the signals with respect to the total height of the instrument vial.

Atomic Force Microscopy (AFM). An MFP-3D-BIO AFM (Oxford Instruments, Asylum research, High Wycombe, UK), equipped with a closed fluid cell operating in AC mode under ambient conditions, and a silicon N type doped OMCL-AC240TS micro cantilever (Olympus, Tokyo, Japan), with a resonance frequency of 70 kHz and a spring constant of 2 N/m, were used to detect and follow the morphology changes of the two model systems.

The samples were first prepared and left to rest for 2 h to ensure a precipitation detection time, that is, the required volume of inhibitor/dispersant was added with a micropipette to a 10 mL sample of freshly prepared model 2 solution. Then, 10 µL aliquots were taken and deposited onto glass probes for sufficient time (<30 min) for the solvents to adequately evaporate. Scanning images of 50 × 50 µm (model 1) and 20 × 20 µm (model 2) were taken and analyzed with Gwyddion® (open-source software, Czech Metrology Institute, Jihlava, Czech Republic) to obtain different morphology descriptor profiles.

3. Results

In this section, results are presented as follows: first, the effect of different *n*-alcanes on the precipitation detection time and aggregation kinetics is shown. Second, the effect of the commercial inhibitors/dispersants on agglomeration dynamics and morphology of deposited layers is assessed. Third, an evaluation of the performance of the commercial products is given from an operational perspective.

3.1. Model 1: Effect of n-Alcanes on Agglomeration Dynamics

As mentioned in the Materials and Methods section, the transmission/backscattering signals are taken by the instrument in 20 µm steps through pulses every 25 s. Samples of model 1 were put into the vials and %ΔBS signals followed for 4 h. Figure 1 shows the normalized height of the sample (where 0 corresponds to the bottom and 1 to the top of the measurement vial) as a function of time for all *n*-alkanes. The changes in height correspond to the evolution of the %ΔBS signal where it is dominant. For example, at the top of the vial, the signal for *n*-dodecane remained constant for approximately 1150 s and the %ΔT signal remained below 0.2 (detection limit of the instrument). After this time, the %ΔBS signal starts to decrease and becomes less dominant while the %ΔT signal starts to increase (e.g., the sample starts to clarify from the top of the vial to the bottom). It can be observed that as time progresses, the signals decrease through different paths. This means that asphaltenes in the freshly prepared samples start to aggregate and precipitate, which means that backscattering will drop from the top of the sample as no obstacles for light are present (noting that backscattering will increase at the bottom of the sample as material accumulates) and the transmission will increase as a consequence of clarification. It can also be noted that as the carbon number (and size) of the *n*-alkane increases, agglomeration kinetics are slowed. This is consistent with previous studies [34,63] where the time required to detect agglomeration (or the precipitation detection time) changes. The observation could be attributed to a coupled effect between an increase in the viscosity of the bulk and reduced diffusivity of asphaltenes. It is important to note that there seem to be two governing regimes depending on the actual concentration of the precipitant: at high concentrations (and the case of this work), solubility decreases as the carbon number decreases, while at low concentrations solubility seems to remain constant [64].

In Figure 1, three different regions can be arbitrarily identified and correlated to the different phenomena present: a stage (i) of initial agglomeration, where the %ΔBS signal tends to remain constant over time; a second stage (ii), where aggregation is sufficient for sedimentation to occur accompanied by a sharp drop in height (conversely, the %ΔT signal increases, an indication of clarification); and a final stage (iii), where precipitated material accumulates at the bottom of the vial and the height stabilizes again (the values of the %ΔBS signal in this region are high due to the accumulated material). The dynamics of these stages can be explained through a balance between gravitational and diffusive forces, normally represented by the Péclet number ($Pe = \frac{3/4\pi\Delta\rho g a^4}{k_B T}$.) which relates these forces in the absence of flow in terms of the radii of the particles (a), the density difference between phases ($\Delta\rho$) and the thermal energy ($k_B T$) [65,66]. During (i), initial agglomeration and subsequent slow sedimentation occur (Pe << 1). Asphaltene-asphaltene interactions are dominated by Van der Waals attraction forces with colloidal structures maintaining mobility (e.g., low-density arrested states and Brownian motion). As the aggregates grow in size, the strength of the gravitational forces increases inducing a fluid phase transition (Pe >> 1, sedimentation

becomes more relevant) from (ii) to (iii). This means that moderate interactions come into play and enhance a colloidal crystallization-type of sediment, all mediated by the differences in carbon number of the precipitant, resulting in denser sediments for systems of low carbon numbers and vice versa [67]. The trend observed during (iii), where the height of dominant %ΔBS is lowest for *n*-hexane and highest for *n*-dodecane, precisely represents the differences in density and the final amount of precipitated material.

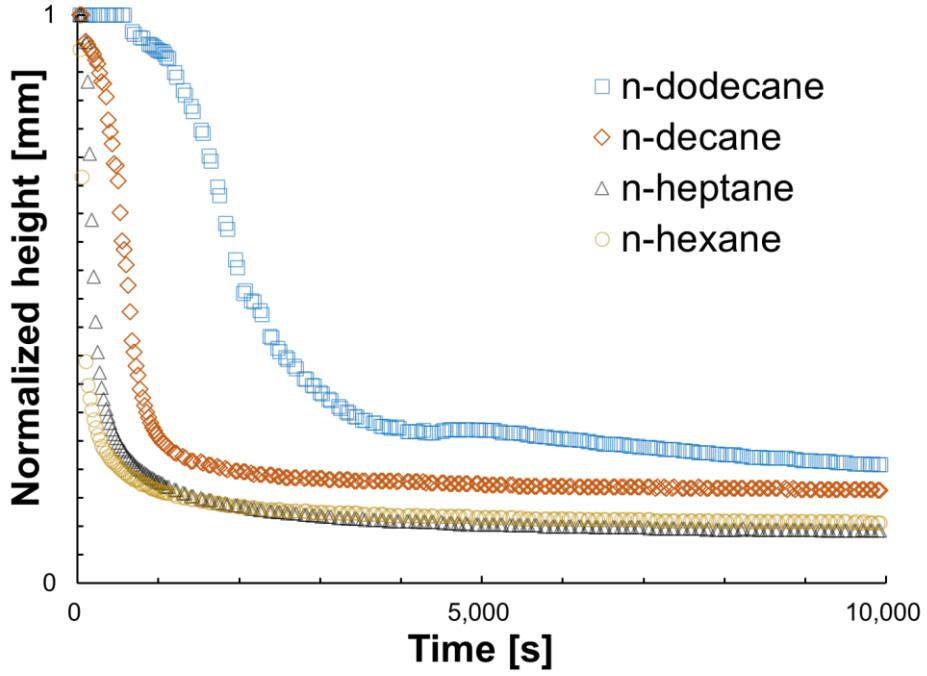

Figure 1. Normalized height as a function of time for the *n*-alkanes used in this work. The shape of the curves matches the shape of the %ΔBS signals in the region where %ΔT is below 0.2.

Similar to other techniques previously mentioned, it is possible to extract certain semi-quantitative parameters from the data in Figure 1 to establish a precipitation detection time. Considering the three regions previously described, Table 3 shows the calculated aggregation time (t_1), that is, the time at which the normalized height starts to drop due to sufficient asphaltene aggregation (the %ΔBS signal is dominant); the sedimentation time (t_2), that is, the time at which the normalized height remains unchanged; the normalized final height of precipitated material (h_d) and the viscosity of all the *n*-alkane solutions.

Table 3. Analysis parameters.

n-Alkane	Aggregation Time (t_1, *s*)	Sedimentation Time (t_2, *s*)	Final Height (h_d, mm)	Viscosity (μ_s, *cP*) *
Dodecane	1150	3875	3.7	1.56
Decane	275	870	3.2	0.93
Heptane	100	400	2.2	0.41
Hexane	25	225	1.8	0.32

* Viscosity values were extracted from [68].

In line with other studies [69–71], the calculated aggregation time (t_1) of Table 3 is consistent with a diffusion-limited cluster aggregation (DLCA) model which corroborates that the viscosity of the solution and attractive forces are responsible for the initial stages of these processes. Figure 2 shows the evolution of the %ΔBS signal as a function of the height of the sample until t_1 is reached for each *n*-alkane. It can be noted that for low carbon numbers, the magnitude of the signal is higher, indicative of an increased size of

material that will eventually sediment faster. Furthermore, the calculated sedimentation time (t_2) increases with the carbon number, suggesting that asphaltene aggregates require more time to precipitate and that the effectiveness of the asphaltene–asphaltene collisions, while the gravitational forces dominate, is higher in precipitants of low carbon number [72]. Table 3 also shows the viscosity of the solutions, extracted from the literature as a reference, and the final height of the precipitated material in the vial. This is to show that these remarks are in line with what has been previously observed; as the viscosity of the media increases with carbon number, diffusivity is slowed and the final precipitated material forms a less-dense layer in the absence of flow.

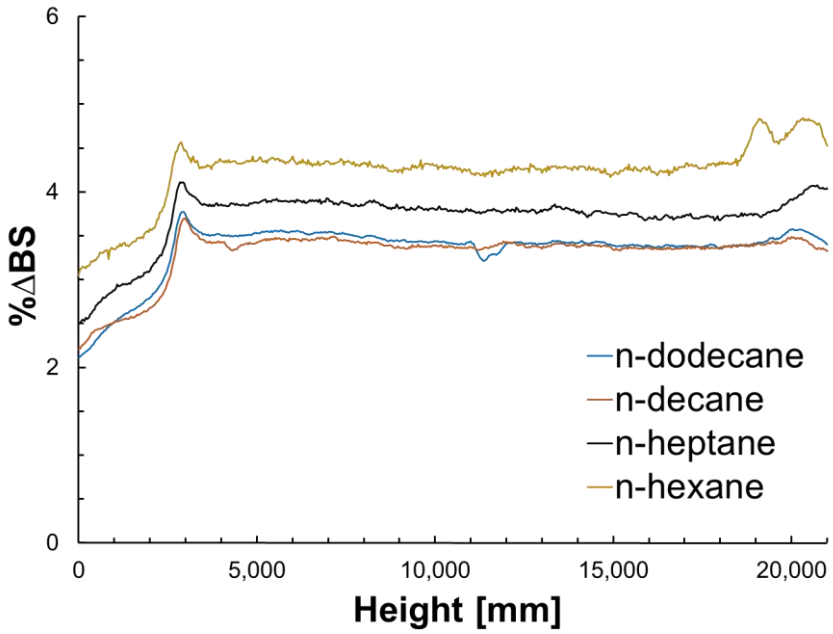

Figure 2. %ΔBS signal as a function of the height of the sample from 0 to t_1 for all n-alkanes.

3.2. Effect of Inhibitors and Dispersants on Model Systems

In order to assess the possible stabilization mechanisms behind inhibition or dispersion through AFM measurements, a fully stable system is needed. This is translated to a system where no asphaltene aggregates or sediments are detected via %ΔBS/%ΔT signals. For this reason, a concentration sweep was performed and the optimal concentration for each additive and for each model system is presented in Table 4. An important aspect of this data is that the ENP additive requires a significantly larger concentration to stabilize the system compared to the others.

Table 4. Concentration of inhibitor/dispersant where both model systems remain stable (no asphaltene aggregation or sedimentation detected).

Additive	Model 1 [g/L]	Model 2 [g/L]
ENP	256	100
DBSA	6	3
APR	0.1	0.1
PIBSA	0.1	0.1

Figures 3 and 4 show the height as a function of the projected length and the morphology of the sediment for model 1 and model 2 after solvent evaporation (*n*-heptane and toluene), respectively. As a baseline for comparison, Figure 5 shows the same variables for asphaltene solutions in toluene. The projected length is an arbitrary path line within the measurement window selected by the AFM software to report the height of the measured

material. These figures serve as a visual confirmation of one of the initial hypotheses, in which depending on the starting solution, the aggregation/sedimentation routes follow different paths. It is clear from the morphology plots that the final states are a result of the heterogeneities and nonuniform distribution of solubility classes (families of compounds) within crude oil. These direct observations are in line with what has been previously described (qualitatively) by association through other techniques [73,74].

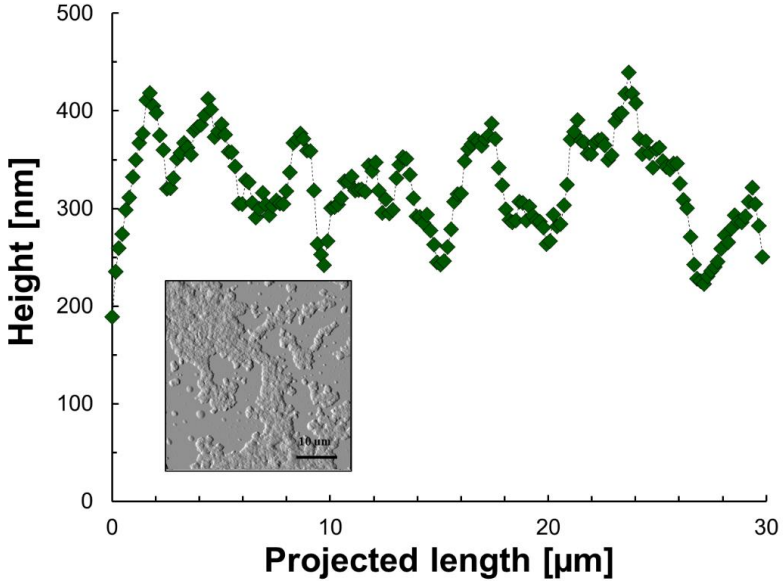

Figure 3. Height as a function of the projected length and morphology of aggregates/sediment of model 1 after *n*-heptane and toluene evaporation. The green icons are the experimental points, the dashed line is for illustrative purposes only and the image is to show the area where data was extracted.

The effects of the inhibitors/dispersants on model 1 and model 2 are shown in Figures 6 and 7, respectively. The average height (AH, a parameter that describes the changes in height of the surface) and the mean square roughness (MSR, a parameter that gives an indication of aggregate size in three dimensions) extracted from the images with Gwyddion® are presented in Table 5. The first aspect to note is that for both model systems, the final conformation is bigger in size (compared to the case without any additive) for APR, whereas similar sizes are obtained for PIBSA. This is evidenced by a higher AH and MSR for APR compared to the reference value at 0% and conversely lower values for PIBSA. This could be an indication of the different phenomena present: larger sizes could represent the action of a dispersant and so the larger aggregate is viewed as a loosely bound asphaltene cluster-dispersant complex that remains soluble. The presence of an aromatic motif on the APR molecule does not provide (which might not be the intended action mechanism) sufficient interaction energy for this compound to bind to the asphaltene cluster. On the other hand, similar/lower sizes could represent the action of an inhibitor, where some monomers are attached to the asphaltene clusters, preventing an increase in their size and further aggregation via active site deactivation (or crowding) and keeping the entire complex fully solubilized [75]. There is evidence from isothermal titration calorimetry (ITC) of similar molecules providing strong interaction energies ($\sim \Delta G = -22$ kJ/mol) with asphaltene model compounds, suggesting H-bonding from the PIBSA molecule and $\pi - \pi$ stacking from the asphaltenes [76,77].

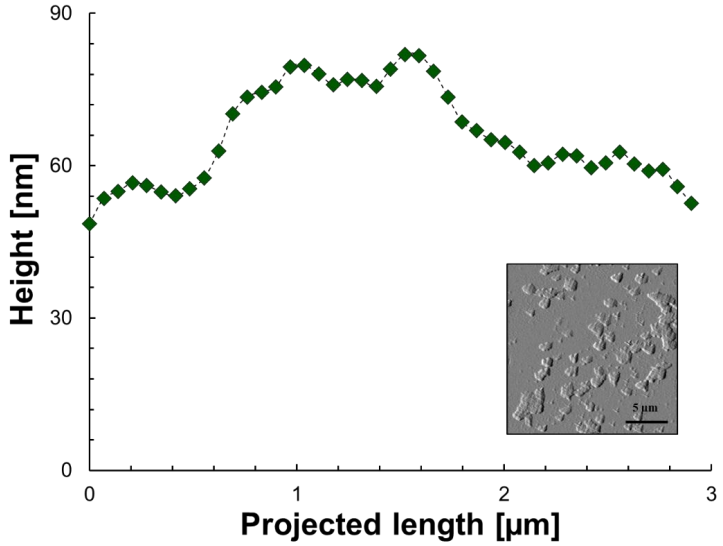

Figure 4. Height as a function of the projected length and morphology of aggregates/sediment of model 2 after *n*-heptane and toluene evaporation. The green icons are the experimental points, the dashed line is for illustrative purposes only and the image is to show the area where data was extracted.

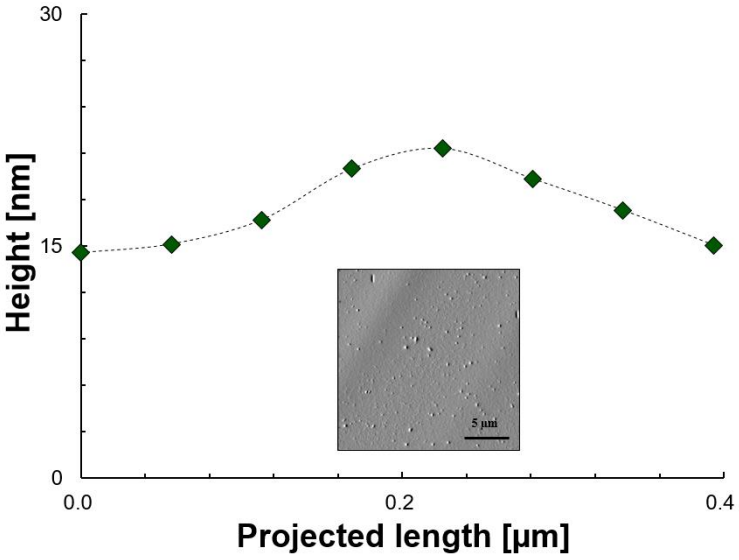

Figure 5. Height as a function of the projected length and morphology of aggregates/sediment of an undisturbed asphaltenes in toluene solution. The green icons are the experimental points, the dashed line is for illustrative purposes only and the image is to show the area where data was extracted.

Table 5. Average height and the mean square roughness for model 1 and model 2 after addition of the inhibitors/dispersants APR and PIBSA and 0% of additive for comparison.

Parameter	Model 1	Model 2
Average height [nm]	0%: 311 APR: 440 PIBSA: 208	0%: 48 APR: 75 PIBSA: 51
Mean square roughness [nm]	0% 42 APR: 65 PIBSA: 30	0%: 11 APR: 13 PIBSA: 7

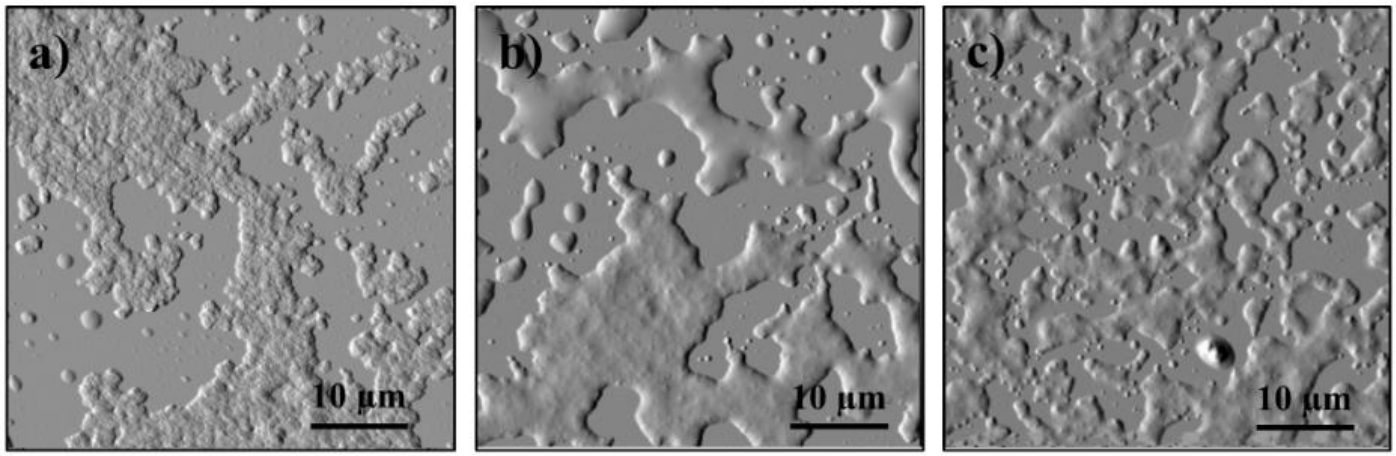

Figure 6. Comparison of the morphology of the resulting (after evaporation) state compared to (**a**) Initial conditions of model 1 after addition of (**b**) APR and (**c**) PIBSA.

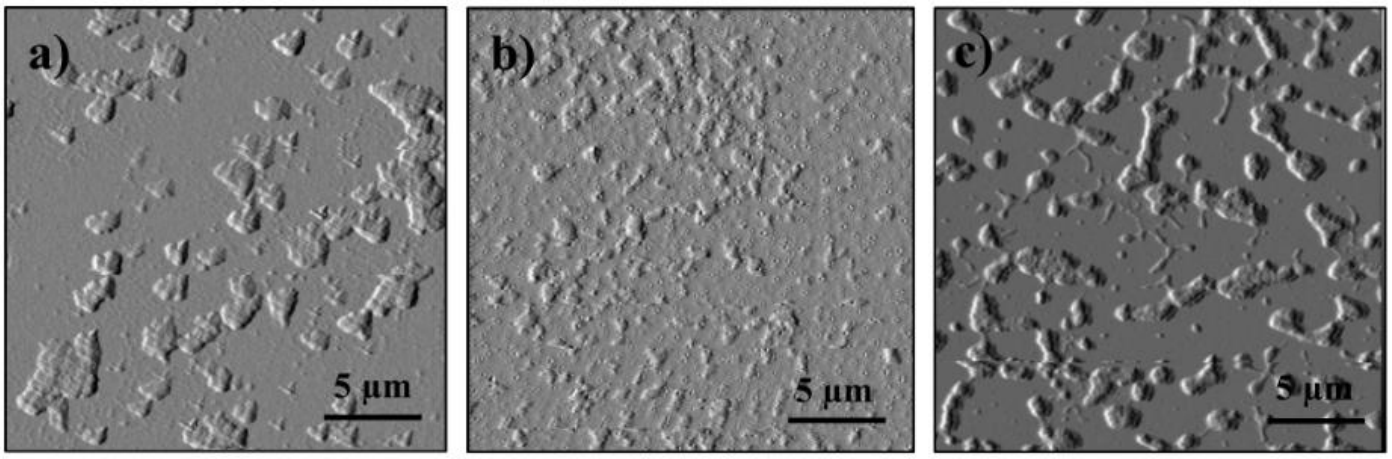

Figure 7. Comparison of the morphology of the resulting (after evaporation) state compared to (**a**) Initial conditions of model 2 after addition of (**b**) APR and (**c**) PIBSA.

3.3. Performance of Inhibitors/Dispersants on Stabilization

To further evaluate the performance of the different chemicals in terms of the stabilization of asphaltene aggregates, data obtained from %ΔBS/%ΔT measurements were analyzed. The Turbiscan stability index (TSI) is a relativistic quantity that takes the sum of the difference between the current value of the signal of interest (h_i) with the previous value (h_{i-1}) and divides it into the total height (H) of the sample $\left(TSI = \frac{(\sum h_i - h_{i-1})}{H}\right)$. This parameter provides an easy-to-use initial approximation of the physical stability of a given system and can be incorporated as a complementary analysis. Figure 8 shows the TSI parameter as a function of time for the inhibitors/dispersants and model 1/model 2. It can be noted that all chemicals perform well in terms of stabilization (a rule of thumb when analyzing these values is that the system is considered as very stable if TSI < 1), which means that the asphaltene aggregates maintained their small size. Within the region of stability, model 1 seems to be more stable than model 2. This is an interesting and expected result. On one hand, model 1 does contain actual crude oil (as well as other compounds), which means that this is the result of an averaged behavior, something that is closer to authentic field operations. On the other hand, in model 2 (extracted asphaltenes), asphaltene interactions are favored. For model 1, no conclusions on whether inhibition or dispersion can be drawn but for model 2, it can be said that PIBSA and DBSA act as

inhibitors and that APR and ENP act as dispersants. These observations are in line with the AFM images obtained in the previous section.

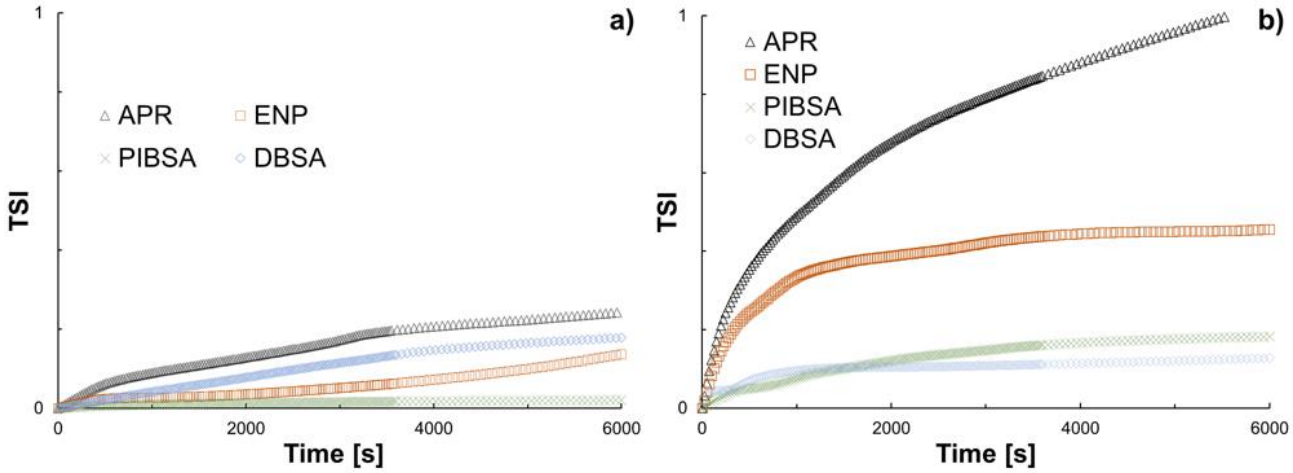

Figure 8. TSI as a function of time for the inhibitors/dispersants acting on (**a**) model 1 and (**b**) model 2.

4. Discussion

The first part of the Results section was dedicated to the effect of various *n*-alkanes on the precipitation detection time of two different models: model 1 (crude oil and solvents) and model 2 (extracted asphaltenes re-solubilized in toluene). The results presented in Figures 1 and 2 show that there is a relationship between the carbon number, the concentration and the precipitation detection time. In line with other studies and consolidating contrasting results, it was shown that the influence of the carbon number on the diffusion and subsequent aggregate growth of asphaltene clusters follows two trends depending on the concentration of the precipitant. At high concentrations (this work), asphaltene solubility is strongly affected when the carbon number decreases, which translates to low carbon numbers, inducing early precipitation. At low concentrations, solubility seems to remain constant, noting that a diffusion limited cluster aggregation (DLCA) model would potentially be adequate to describe this process. Furthermore, an assessment of the precipitated material was made, suggesting that besides influencing the solubility of asphaltene clusters, the carbon number of the precipitant also influences the density of the sediment. The implications in terms of operations of these observations could mean that targeted chemical treatments could be developed, and specific chemistries based on simple parameters could be implemented to prevent sedimentation. Further analysis with the incorporation of favorable solubility conditions (e.g., a mix between alkanes and aromatics) could aid in fine-tuning certain aspects for chemical treatment development.

One of the precipitants (i.e., *n*-heptane) was selected to further analyze the effect of inhibitors/dispersants on the precipitation detection time. The terms inhibitor and dispersant can sometimes be ambiguous. Here, an attempt was made to separate these terms and relate them to physical mechanisms. Inhibition is to be understood as a mechanism through which active sites are blocked (either through adsorption or any type of interaction) and further aggregation is not possible because other asphaltene monomers or clusters do not have access to such sites. On the other hand, dispersion is to be understood as a mechanism where interactions are not the main channel for precipitation prevention but instead, the steric barriers (e.g., a type of polymeric network) that are created by the long chains of the additives do not allow the asphaltene clusters/monomers to interact with one another.

AFM imaging was used to assess the extent of aggregation and subsequent precipitation of model 1 and model 2 under the influence of commercially available chemical additives normally used as part of the multiple strategies for flow assurance (Figures 3–7). In this case, only one of the inhibitors (PIBSA) and one of the dispersants (APR) were used. Results indicated that the inhibitor produced final states (AH and MSR after evaporation)

that are smaller in size compared to the system without additives, which means that the inhibitor is capable of reducing the density of the formed complex and prevents it from further growth. Similarly, the dispersant produced final states greater in size compared to the system without additive, suggesting a type of thickening of the media which could hinder cluster mobility, hence further aggregation.

A final evaluation was performed through transmission/backscattering signal analysis on all the additives proposed in this work and both model systems. Figure 8 shows the main results, corroborating the initial hypotheses and the possible action mechanisms behind inhibition and dispersion. Dispersants, even though yielding an increased size of the evaluated system, prevent sedimentation (and deposition if under flow) to the same extent as inhibitors. The decision in terms of operations would therefore be made based on other aspects such as economic feasibility, product availability (supply), ease of implementation (depending on vendor specifications for application) and sustainability. Based on the results of this work, a point could be made on which additives would be the preferred choice. For this particular case (i.e., a heavy crude oil of high acidity, high asphaltene content and low saturates content) and considering the previously mentioned aspects, the suggestion would be to use APR as a dispersant and PIBSA as an inhibitor. Dispersion has the added value of potentially ensuring that other problematic fractions (e.g., saturates) sensible to pressure-temperature changes do not get a nucleation point for growth, whereas inhibition could prevent large plug formation. Both systems presented with TSI < 1, a low dosage for high efficiency and a long-term physical stability. These are key positive variables, operationally speaking.

This work focused on asphaltenes mainly because severe operational issues are largely attributed to this fraction of crude oil. However, complex problems can arise when other components negatively interact with pressure-temperature changes (hydrates, scales) and should therefore be included in future studies.

Author Contributions: Conceptualization, D.M., M.A., O.A., and D.P.; methodology, D.M., O.A., D.P; validation, D.M., M.A., O.A., and D.P.; formal analysis, D.M., D.P.; investigation, D.M.; data curation, D.M., O.A., D.P.; writing—original draft preparation, D.M., M.A., O.A., and D.P.; writing—review and editing, D.M., M.A., O.A., and D.P.; supervision, M.A., O.A., D.P. All authors have read and agreed to the published version of the manuscript.

Funding: This research received no external funding.

Data Availability Statement: Not applicable.

Conflicts of Interest: The authors declare no conflict of interest.

References

1. Harbottle, D.; Chen, Q.; Moorthy, K.; Wang, L.; Xu, S.; Liu, Q.; Sjoblom, J.; Xu, Z. Problematic Stabilizing Films in Petroleum Emulsions: Shear Rheological Response of Viscoelastic Asphaltene Films and the Effect on Drop Coalescence. *Langmuir* **2014**, *30*, 6730–6738. [CrossRef] [PubMed]
2. Kuznicki, N.P.; Harbottle, D.; Masliyah, J.H.; Xu, Z. Probing Mechanical Properties of Water–Crude Oil Interfaces and Colloidal Interactions of Petroleum Emulsions Using Atomic Force Microscopy. *Energy Fuels* **2017**, *31*, 3445–3453. [CrossRef]
3. Hjartnes, T.N.; Sørland, G.H.; Simon, S.; Sjöblom, J. Demulsification of Crude Oil Emulsions Tracked by Pulsed Field Gradient (PFG) Nuclear Magnetic Resonance (NMR). Part I: Chemical Demulsification. *Ind. Eng. Chem. Res.* **2019**, *58*, 2310–2323. [CrossRef]
4. Ivanova, N.O.; Xu, Z.; Liu, Q.; Masliyah, J.H. Surface forces in unconventional oil processing. *Curr. Opin. Colloid Interface Sci.* **2017**, *27*, 63–73. [CrossRef]
5. Foudazi, R.; Qavi, S.; Masalova, I.; Malkin, A.Y. Physical chemistry of highly concentrated emulsions. *Adv. Colloid Interface Sci.* **2015**, *220*, 78–91. [CrossRef]
6. Schuler, B.; Meyer, G.; Peña, D.; Mullins, O.C.; Gross, L. Unraveling the Molecular Structures of Asphaltenes by Atomic Force Microscopy. *J. Am. Chem. Soc.* **2015**, *137*, 9870–9876. [CrossRef]
7. Bridot, J.-L.; Langevin, D.; Mullins, O.C. Role of Asphaltene Origin in Its Adsorption at Oil–Water Interfaces. *Energy Fuels* **2022**, *36*, 8749–8759. [CrossRef]
8. Zahabi, A.; Gray, M.R.; Dabros, T. Kinetics and Properties of Asphaltene Adsorption on Surfaces. *Energy Fuels* **2012**, *26*, 1009–1018. [CrossRef]

9. Rane, J.P.; Harbottle, D.; Pauchard, V.; Couzis, A.; Banerjee, S. Adsorption kinetics of asphaltenes at the oil-water interface and nanoaggregation in the bulk. *Langmuir* **2012**, *28*, 9986–9995. [CrossRef]
10. Maqbool, T.; Srikiratiwong, P.; Fogler, H.S. Effect of Temperature on the Precipitation Kinetics of Asphaltenes. *Energy Fuels* **2011**, *25*, 694–700. [CrossRef]
11. Martins, R.G.; Martins, L.S.; Santos, R.G. Effects of Short-Chain n-Alcohols on the Properties of Asphaltenes at Toluene/Air and Toluene/Water Interfaces. *Colloids Interfaces* **2018**, *2*, 13. [CrossRef]
12. Hart, A. A review of technologies for transporting heavy crude oil and bitumen via pipelines. *J. Pet. Explor. Prod. Technol.* **2014**, *4*, 327–336. [CrossRef]
13. Speight, J.G. Exploration, Recovery, and Transportation. In *The Chemistry and Technology of Petroleum*; CRC Press, Taylor and Francis Group, LLC: Boca Raton, FL, USA, 2007.
14. Martínez-Palou, R.; Mosqueira, M.D.L.; Zapata-Rendón, B.; Mar-Juárez, E.; Bernal-Huicochea, C.; Clavel-López, J.d.l.C.; Aburto, J. Transportation of heavy and extra-heavy crude oil by pipeline: A review. *J. Pet. Sci. Eng.* **2011**, *75*, 274–282. [CrossRef]
15. Saniere, A.; Hénaut, I.; Argillier, J.F. Pipeline transportation of heavy oils, a strategic, economic and technological challenge. *Oil Gas Sci. Technol.* **2004**, *59*, 455–466. [CrossRef]
16. Buckley, J.S. Asphaltene Deposition. *Energy Fuels* **2012**, *26*, 4086–4090. [CrossRef]
17. Buenrostro-Gonzalez, E.; Lira-Galeana, C.; Gil-Villegas, A.; Wu, J. Asphaltene precipitation in crude oils: Theory and experiments. *AIChE J.* **2004**, *50*, 2552–2570. [CrossRef]
18. Hoepfner, M.P.; Limsakoune, V.; Chuenmeechao, V.; Maqbool, T.; Fogler, H.S. A Fundamental Study of Asphaltene Deposition. *Energy Fuels* **2013**, *27*, 725–735. [CrossRef]
19. Hoepfner, M.P.; Vilas Bôas Fávero, C.; Haji-Akbari, N.; Fogler, H.S. The Fractal Aggregation of Asphaltenes. *Langmuir* **2013**, *29*, 8799–8808. [CrossRef]
20. Pradilla, D.; Subramanian, S.; Simon, S.; Sjöblom, J.; Beurroies, I.; Denoyel, R. Microcalorimetry Study of the Adsorption of Asphaltenes and Asphaltene Model Compounds at the Liquid-Solid Surface. *Langmuir* **2016**, *32*, 7294–7305. [CrossRef]
21. Vargas, F.M.; Creek, J.L.; Chapman, W.G. On the Development of an Asphaltene Deposition Simulator. *Energy Fuels* **2010**, *24*, 2294–2299. [CrossRef]
22. Tavakkoli, M.; Panuganti, S.R.; Vargas, F.M.; Taghikhani, V.; Pishvaie, M.R.; Chapman, W.G. Asphaltene Deposition in Different Depositing Environments: Part 1. Model Oil. *Energy Fuels* **2014**, *28*, 1617–1628. [CrossRef]
23. Campen, S.; di Mare, L.; Smith, B.; Wong, J.S.S. Determining the Kinetics of Asphaltene Adsorption from Toluene: A New Reaction–Diffusion Model. *Energy Fuels* **2017**, *31*, 9101–9116. [CrossRef]
24. Elkhatib, O.; Chaisoontornyotin, W.; Gesho, M.; Goual, L. Nanoscale Investigation of Asphaltene Deposition under Capillary Flow Conditions. *Energy Fuels* **2020**, *34*, 5148–5158. [CrossRef]
25. Torkaman, M.; Bahrami, M.; Dehghani, M. Influence of Temperature on Aggregation and Stability of Asphaltenes. I. Perikinetic Aggregation. *Energy Fuels* **2017**, *31*, 11169–11180. [CrossRef]
26. Torkaman, M.; Bahrami, M.; Dehghani, M.R. Influence of Temperature on Aggregation and Stability of Asphaltenes. II. Orthokinetic Aggregation. *Energy Fuels* **2018**, *32*, 6144–6154. [CrossRef]
27. Sharma, A.; Groenzin, H.; Tomita, A.; Mullins, O.C. Probing Order in Asphaltenes and Aromatic Ring Systems by HRTEM. *Energy Fuels* **2002**, *16*, 490–496. [CrossRef]
28. Sharma, A.; Mullins, O.C. Insights into Molecular and Aggregate Structures of Asphaltenes Using HRTEM. In *Asphaltenes, Heavy Oils, and Petroleomics*; Mullins, O.C., Ed.; Springer: New York, NY, USA, 2007; pp. 205–229.
29. Trejo, F.; Ancheyta, J.; Rana, M.S. Structural Characterization of Asphaltenes Obtained from Hydroprocessed Crude Oils by SEM and TEM. *Energy Fuels* **2009**, *23*, 429–439. [CrossRef]
30. Goual, L.; Zhang, B.; Rahham, Y. Nanoscale Characterization of Thin Films at Oil/Water Interfaces and Implications to Emulsion Stability. *Energy Fuels* **2021**, *35*, 444–455. [CrossRef]
31. Elkhatib, O.; Zhang, B.; Goual, L. New Insights into Asphaltene Structure and Aggregation by High-Resolution Microscopy. *Energy Fuels* **2022**, *36*, 8692–8700. [CrossRef]
32. Morita, T.; Morimoto, M.; Shibuta, S.; Imamura, H.; Yamamoto, H.; Tykwinski, R.R.; Scott, D.E.; Stryker, J.M.; Suzuki, T.; Tanaka, R. Disaggregation of Asphaltene Aggregates in Solutions Depending upon Affinity Indices of the Hansen Solubility Parameter Using Ultrasmall-, Small-, and Wide-Angle X-ray Scattering. *Energy Fuels* **2022**, *36*, 10043–10051. [CrossRef]
33. Cassiède, M.; Mejia, A.; Radji, S.; Carrier, H.; Daridon, J.-L.; Saidoun, M.; Tort, F. Evaluation of the Influence of a Chemical Inhibitor on Asphaltene Destabilization and Deposition Mechanisms under Atmospheric and Oil Production Conditions Using QCM and AFM Techniques. *Energy Fuels* **2021**, *35*, 17551–17565. [CrossRef]
34. Chaisoontornyotin, W.; Haji-Akbari, N.; Fogler, H.S.; Hoepfner, M.P. Combined Asphaltene Aggregation and Deposition Investigation. *Energy Fuels* **2016**, *30*, 1979–1986. [CrossRef]
35. Haji-Akbari, N.; Masirisuk, P.; Hoepfner, M.P.; Fogler, H.S. A Unified Model for Aggregation of Asphaltenes. *Energy Fuels* **2013**, *27*, 2497–2505. [CrossRef]
36. Tavakkoli, M.; Panuganti, S.R.; Taghikhani, V.; Pishvaie, M.R.; Chapman, W.G. Asphaltene Deposition in Different Depositing Environments: Part 2. *Real Oil. Energy Fuels* **2014**, *28*, 3594–3603. [CrossRef]
37. Spiecker, P.M.; Kilpatrick, P.K. Interfacial Rheology of Petroleum Asphaltenes at the Oil−Water Interface. *Langmuir* **2004**, *20*, 4022–4032. [CrossRef]

38. Speight, J.G. Chapter 11: Asphaltene Constituents. In *The Chemistry and Technology of Petroleum*; CRC Press: Boca Raton, FL, USA; Taylor & Francis Group: Abingdon, UK, 2007; pp. 315–344.
39. Zhang, Y.; Siskin, M.; Gray, M.R.; Walters, C.C.; Rodgers, R.P. Mechanisms of Asphaltene Aggregation: Puzzles and a New Hypothesis. *Energy Fuels* **2020**, *34*, 9094–9107. [CrossRef]
40. Maqbool, T.; Balgoa, A.T.; Fogler, H.S. Revisiting Asphaltene Precipitation from Crude Oils: A Case of Neglected Kinetic Effects. *Energy Fuels* **2009**, *23*, 3681–3686. [CrossRef]
41. Wang, J.; Buckley, J.S. Asphaltene Stability in Crude Oil and Aromatic SolventsThe Influence of Oil Composition. *Energy Fuels* **2003**, *17*, 1445–1451. [CrossRef]
42. Hammami, A.; Ratulowski, J. Chapter 23. Precipitation and Deposition of Asphaltenes in Production Systems: A Flow Assurance Overview. In *Asphaltenes, Heavy Oils, and Petroleomics*; Mullins, O., Sheu, E., Hammani, A., Marshall, A., Eds.; Springer, LLC: Berlin/Heidelberg, Germany, 2007.
43. Haji-Akbari, N.; Teeraphapkul, P.; Fogler, H.S. Effect of Asphaltene Concentration on the Aggregation and Precipitation Tendency of Asphaltenes. *Energy Fuels* **2014**, *28*, 909–919. [CrossRef]
44. Haji-Akbari, N.; Teeraphapkul, P.; Balgoa, A.T.; Fogler, H.S. Effect of n-Alkane Precipitants on Aggregation Kinetics of Asphaltenes. *Energy Fuels* **2015**, *29*, 2190–2196. [CrossRef]
45. Maqbool, T.; Raha, S.; Hoepfner, M.P.; Fogler, H.S. Modeling the Aggregation of Asphaltene Nanoaggregates in Crude Oil−Precipitant Systems. *Energy Fuels* **2011**, *25*, 1585–1596. [CrossRef]
46. Lawal, K.A.; Crawshaw, J.P.; Boek, E.S.; Vesovic, V. Experimental Investigation of Asphaltene Deposition in Capillary Flow. *Energy Fuels* **2012**, *26*, 2145–2153. [CrossRef]
47. Nabzar, L.; Aguiléra, M.E. The Colloidal Approach. A Promising Route for Asphaltene Deposition Modelling. *Oil Gas Sci. Technol. -Rev. IFP* **2008**, *63*, 21–35. [CrossRef]
48. Eskin, D.; Ratulowski, J.; Akbarzadeh, K.; Pan, S. Modelling asphaltene deposition in turbulent pipeline flows. *Can. J. Chem. Eng.* **2011**, *89*, 421–441. [CrossRef]
49. Campen, S.; Moorhouse, S.J.; Wong, J.S.S. Mechanism of an asphaltene inhibitor in different depositing environments: Influence of colloid stability. *J. Pet. Sci. Eng.* **2020**, *184*, 106502. [CrossRef]
50. Khaleel, A.T.; Sisco, C.J.; Tavakkoli, M.; Vargas, F.M. An Investigation of the Effect of Asphaltene Polydispersity on Asphaltene Precipitation and Deposition Tendencies. *Energy Fuels* **2022**, *36*, 8799–8808. [CrossRef]
51. Cheraghian, G.; Wistuba, M.P.; Kiani, S.A. Behnood, M. Afrand, and A.R. Barron, Engineered nanocomposites in asphalt binders. *Nanotechnol. Rev.* **2022**, *11*, 1047–1067. [CrossRef]
52. Hu, C.; Hartman, R.L. High-throughput packed-bed microreactors with in-line analytics for the discovery of asphaltene deposition mechanisms. *AIChE J.* **2014**, *60*, 3534–3546. [CrossRef]
53. Goual, L.; Sedghi, M.; Wang, X.; Zhu, Z. Asphaltene Aggregation and Impact of Alkylphenols. *Langmuir* **2014**, *30*, 5394–5403. [CrossRef]
54. Goual, L.; Sedghi, M. Role of ion-pair interactions on asphaltene stabilization by alkylbenzenesulfonic acids. *J. Colloid Interface Sci.* **2015**, *440*, 23–31. [CrossRef]
55. Institute, E. IP 469: Determination of saturated, aromatic and polar compounds in petroleum products by thin layer chromatography and flame ionization detection. In *IP Test Methods*; Energy Institute: London, UK, 2006.
56. *ASTM D7042-19*; Standard Test Method for Dynamic Viscosity and Density of Liquids by Stabinger Viscometer and the Calculation of Kinematic Viscosity. ASTM International: West Conshohocken, PA, USA, 2019.
57. *ASTM D664-18e2*; Standard Test Method for Acid Number of Petroleum Products by Potentiometric Titration. ASTM International: West Conshohocken, PA, USA, 2018.
58. *ASTM D6560-17*; Test Method for Determination of Asphaltenes (Heptane Insolubles) in Crude Petroleum and Petroleum Products. ASTM International: West Conshohocken, PA, USA, 2017.
59. Wiehe, I.A. Asphaltene Solubility and Fluid Compatibility. *Energy Fuels* **2012**, *26*, 4004–4016. [CrossRef]
60. Alboudwarej, H.; Akbarzadeh, K.; Beck, J.; Svrcek, W.Y.; Yarranton, H.W. Regular Solution Model for Asphaltene Precipitation from Bitumens and Solvents. *AIChE J.* **2003**, *49*, 2948–2956. [CrossRef]
61. Wiehe, I.A.; Yarranton, H.W.; Akbarzadeh, K.; Rahimi, P.M.; Teclemariam, A. The Paradox of Asphaltene Precipitation with Normal Paraffins. *Energy Fuels* **2005**, *19*, 1261–1267. [CrossRef]
62. Manek, M.B. Asphaltene Dispersants as Demulsification Aids. In *SPE International Symposium on Oilfield Chemistry*; Society of Petroleum Engineers, USA: San Antonio, TX, USA, 1995; p. SPE-28972-MS.
63. González, G.; Acevedo, S.; Castillo, J.; Villegas, O.; Ranaudo, M.A.; Guzmán, K.; Orea, M.; Bouyssiere, B. Study of Very High Molecular Weight Cluster Presence in THF Solution of Asphaltenes and Subfractions A1 and A2, by Gel Permeation Chromatography with Inductively Coupled Plasma Mass Spectrometry. *Energy Fuels* **2020**, *34*, 12535–12544. [CrossRef]
64. Mitchell, D.L.; Speight, J.G. The solubility of asphaltenes in hydrocarbon solvents. *Fuel* **1973**, *52*, 149–152. [CrossRef]
65. Lee, M.H.; Furst, E.M. Formation and evolution of sediment layers in an aggregating colloidal suspension. *Phys. Rev. E* **2006**, *74*, 031401. [CrossRef]
66. Whitmer, J.K.; Luijten, E. Sedimentation of aggregating colloids. *J. Chem. Phys.* **2011**, *134*, 034510. [CrossRef]
67. Dong, K.J.; Yang, R.Y.; Zou, R.P.; Yu, A.B. Role of Interparticle Forces in the Formation of Random Loose Packing. *Phys. Rev. Lett.* **2006**, *96*, 145505. [CrossRef]

68. Dymond, J.H.; O/ye, H.A. Viscosity of Selected Liquid n-Alkanes. *J. Phys. Chem. Ref. Data* **1994**, *23*, 41–53. [CrossRef]
69. Poozesh, A.; Sharifi, M.; Fahimpour, J. Modeling of Asphaltene Deposition Kinetics. *Energy Fuels* **2020**, *34*, 9304–9319. [CrossRef]
70. Vilas Bôas Fávero, C.; Hanpan, A.; Phichphimok, P.; Binabdullah, K.; Fogler, H.S. Mechanistic Investigation of Asphaltene Deposition. *Energy Fuels* **2016**, *30*, 8915–8921. [CrossRef]
71. Wang, X.; Gu, Y. Characterization of Precipitated Asphaltenes and Deasphalted Oils of the Medium Crude Oil-CO_2 and Medium Crude Oil-n-Pentane Systems. *Energy Fuels* **2011**, *25*, 5232–5241. [CrossRef]
72. Qiao, P.; Harbottle, D.; Li, Z.; Tang, Y.; Xu, Z. Interactions of Asphaltene Subfractions in Organic Media of Varying Aromaticity. *Energy Fuels* **2018**, *32*, 10478–10485. [CrossRef]
73. Syunyaev, R.Z.; Balabin, R.M.; Akhatov, I.S.; Safieva, J.O. Adsorption of Petroleum Asphaltenes onto Reservoir Rock Sands Studied by Near-Infrared (NIR) Spectroscopy. *Energy Fuels* **2009**, *23*, 1230–1236. [CrossRef]
74. Balabin, R.M.; Syunyaev, R.Z.; Schmid, T.; Stadler, J.; Lomakina, E.I.; Zenobi, R. Asphaltene Adsorption onto an Iron Surface: Combined Near-Infrared (NIR), Raman, and AFM Study of the Kinetics, Thermodynamics, and Layer Structure. *Energy Fuels* **2011**, *25*, 189–196. [CrossRef]
75. León, O.; Rogel, E.; Urbina, A.; Andújar, A.; Lucas, A. Study of the adsorption of alkyl benzene-derived amphiphiles on asphaltene particles. *Langmuir* **1999**, *15*, 7653–7657. [CrossRef]
76. Simon, S.; Wei, D.; Barriet, M.; Sjöblom, J. An ITC and NMR study of interaction and complexation of asphaltene model compounds in apolar solvent I: Self-association pattern. *Colloids Surf. A Physicochem. Eng. Asp.* **2016**, *494*, 108–115. [CrossRef]
77. Wei, D.; Simon, S.; Barriet, M.; Sjöblom, J. An ITC study of interaction and complexation of asphaltene model compounds in apolar solvent II: Interactions with asphaltene inhibitors. *Colloids Surf. A Physicochem. Eng. Asp.* **2016**, *495*, 87–99. [CrossRef]